

DRAG REDUCTION IN TURBULENT BOUNDARY LAYERS: EFFECT OF UNIFORM BLOWING AND SUCTION

Y. Kametani^{1,2}, K. Fukagata¹, R. Örlü² and P. Schlatter²

¹ *Dept. of Mechanical Engineering, Keio Univ., Hiyoshi 3-14-1, Yokohama 223-8522, Japan*

² *Linné FLOW Centre, KTH Mechanics, Osquars Backe 18, SE-100 44 Stockholm, Sweden*

yukinori.kametani@mech.kth.se

1 Introduction

The skin friction drag originating from fluid viscosity on surfaces of vehicles has a large impact on environment and economy from the viewpoint of fuel consumption. Due to the laminar-turbulent transition within boundary layers, the skin friction drag increases drastically compared to its laminar counterpart. In order to reduce the skin friction drag, various drag reducing methods have been devised. Soon after the advent of the direct numerical simulation (DNS) of a turbulent channel flow by Kim et al. (1987), numerical studies on drag reduction by riblets (Choi et al., 1993), surfactants (White and Mungal 2008), superhydrophobic surfaces (Türk et al., 2014), active opposition control (Choi et al., 1994), wall-oscillation (Ricco & Quadrio, 2008), and wall deformation (Tomiyama & Fukagata, 2013) in internal flows have been pursued. When it comes to external flows, however, there remains still a need for further investigations.

Another way of modifying the flow is through blowing and suction as *e.g.* employed for film-cooling of turbine blades and slotted wings. Kametani & Fukagata (2011) performed a DNS of a spatially developing turbulent boundary layer (STBL) with uniform blowing from the wall. They found that with blowing at only 0.1% of the freestream velocity one can achieve over 10% drag reduction. Furthermore, high control efficiency is demonstrated: higher net-energy saving rate and gain are achieved compared with different alternative drag reduction controls. As identified from the decomposition of skin friction drag (FIK identity; Fukagata et al., 2002), the wall-flux from the wall can be a strong reduction factor of the skin friction drag, while it enhances the Reynolds shear stress. These results, however, are from a low Reynolds number of around $Re_\tau = 180$, where the flow is not representative of a turbulent boundary layer, and results can hence not be extrapolated to higher, more practical, Reynolds numbers.

Since the first DNS of a STBL by Spalart (1988), the turbulent structures in STBL have been numerically investigated (Robinson, 1991). Due to the recent increase of computing performance, the vortical com-

position of fully developed turbulent boundary layers have been confirmed through DNS, see *e.g.* Sillero et al. (2013), Pirozzoli and Bernardini (2013), and more recently Schlatter et al. (2014). In order to investigate the turbulent structures at higher Reynolds number, Eitel-Amor et al. (2014) performed a large-eddy simulation (LES) at relatively high Reynolds number (up to $Re_\theta = 8000$) and the turbulent structures are investigated through spectral analysis.

In the present study, a LES of a spatially evolving boundary layer with uniform wall transpiration is performed in order to investigate the effect of blowing and suction on the turbulence statistics and primarily on the skin-friction drag and its decomposition at moderate Reynolds number. Aiming at the practical application, the control efficiency is also discussed.

2 Numerical set-up

The governing equations are the incompressible continuity and Navier-Stokes equations. The present large-eddy simulation uses the ADM-RT model (Schlatter et al., 2004). The momentum equation for the resolved velocity \bar{u}_i and pressure \bar{p} is written as

$$\frac{\partial \bar{u}_i}{\partial t} = -\bar{u}_j \frac{\partial \bar{u}_i}{\partial x_j} - \frac{\partial \bar{p}}{\partial x_i} + \frac{1}{Re} \frac{\partial^2 \bar{u}_i}{\partial x_j \partial x_j} - \chi H_N * \bar{u}_i. \quad (1)$$

The equations are non-dimensionalized by the free-stream velocity U_∞ and the inlet displacement thickness, δ_0^* , *i.e.* the computational Reynolds number is defined as $Re = U_\infty \delta_0^* / \nu = 450$, where ν denotes the kinematic viscosity. The relaxation term $\chi H_N * \bar{u}_i$ is based on a high-order three-dimensional filter operation where $H_N \equiv (I - G)^{N+1}$ convoluted with \bar{u}_i . G is a lower-order, low-pass filter. The computational domain is $L_x \times L_y \times L_z = 3000 \times 100 \times 960$ with $N_x \times N_y \times N_z = 2048 \times 257 \times 1536$ spectral collocation points in the streamwise, the wall-normal, and the spanwise directions, respectively. In the physical space, the number of grid points in the streamwise and the spanwise directions increases by a factor of 3/2 due to the dealiasing. The maximum grid resolution in wall units is $\Delta x^+ \times \Delta y_{max}^+ \times \Delta z^+ = 20.9 \times 13.3 \times 8.9$. The boundary layer starts from Blasius profile at the

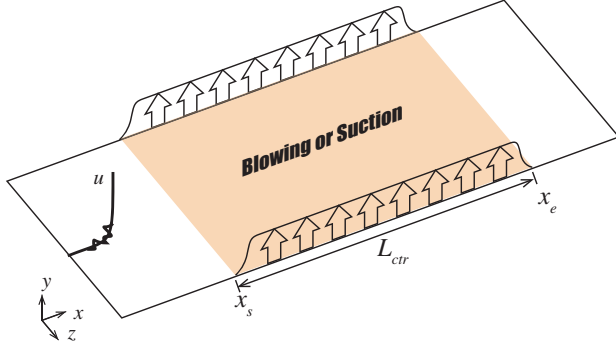


Figure 1: Employed coordinate system and schematic of controlled region.

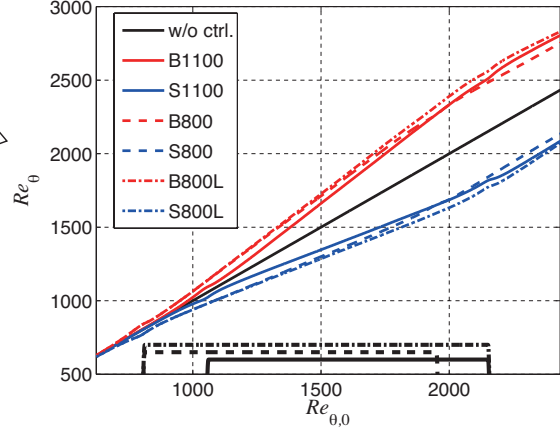


Figure 2: Reynolds number relation.

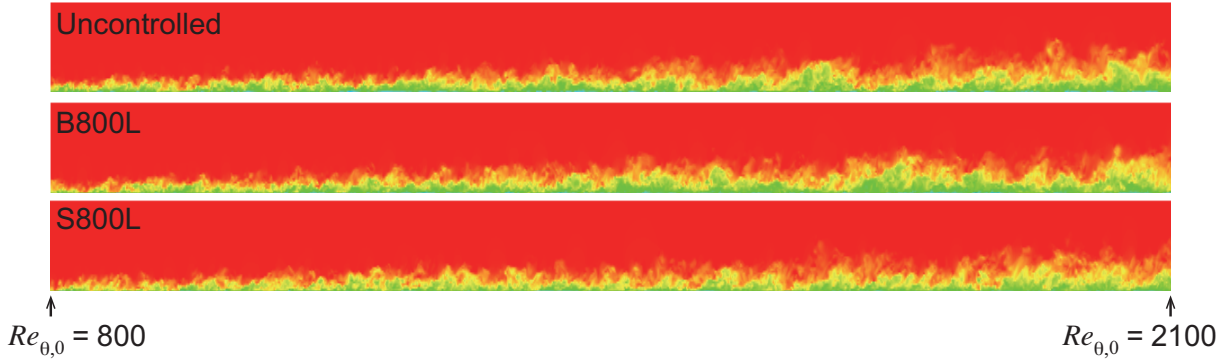


Figure 3: Instantaneous streamwise velocity on the controlled region in $x - y$ plane. The representation is stretched by a factor of 2 in the wall-normal direction.

inlet of the computational domain and transitions to a turbulent boundary layer via a tripping force (detailed in Schlatter et al, 2004 and Schlatter and Örlü, 2012). The boundary layer can be considered turbulent in the range of $Re_\theta > 700$.

Uniform blowing or suction is applied as the wall-boundary condition for the normal velocity, $V_w = \pm 1.0 \times 10^{-3}$, as shown in Fig. 1. Aiming at investigating the area-dependency of the controls, blowing or suction is applied in three different areas: control at $800 < Re_{\theta,0} < 1800$ is referred to as B/S800, $1100 < Re_{\theta,0} < 2100$ as B/S1100 and $800 < Re_{\theta,0} < 2100$ as B/S800L, respectively. The subscript 0 refers to the uncontrolled (reference) case. The averaging time in wall units for computing statistics is $T^+ \approx 2000$ for the uncontrolled case and B/S1100, and $T^+ \approx 1000$ for the other cases.

3 Uniform blowing/suction

The Reynolds number based on the momentum thickness in each case is plotted in Fig. 2 as a function of the streamwise location. The figure shows that the spatial growth of the boundary layer is promoted by blowing and delayed by suction. Although the amplitude of blowing or suction is small, the thickness of the boundary layer in the blowing case is approximately 13% larger than that of the uncontrolled flow at $Re_\theta = 2100$, while it is approximately 18% lower

in the suction case. Instantaneous streamwise velocities of B/S800L are shown in Fig. 3. The promoted development by blowing and delayed one by suction can visually be confirmed.

The statistics at some streamwise locations from B/S1100 are considered next. Figure 4 shows the mean streamwise velocity scaled by local wall units. While the linear law can be found in all cases, the logarithmic profile is not appropriate for the blowing and suction cases. The profiles of the root-mean-square (RMS) of the streamwise, wall-normal and spanwise velocity fluctuations scaled by local wall units are plotted in Fig. 5. Due to the reduced skin friction coefficient, the RMSs are increased by blowing, while those are decreased by the enhanced skin friction in the suction case. The profiles in the suction case indicate their collapse on one curve in the inner region. In the blowing case, the peak values increase downstream faster than those of the uncontrolled case and their locations are at a slightly larger distance from the wall, while the suction case has the opposite trends. It can be concluded that the intensity of the outer-layer structures are effectively reduced by the weak amount of suction.

Similarly, the Reynolds shear stress (RSS) is plotted in Fig. 6. The profiles show that the peak of RSS scaled by the local wall units is gradually increased to over 1.3 in the blowing case, while it is decreased to around 0.6 in the suction case. By inner scaling with

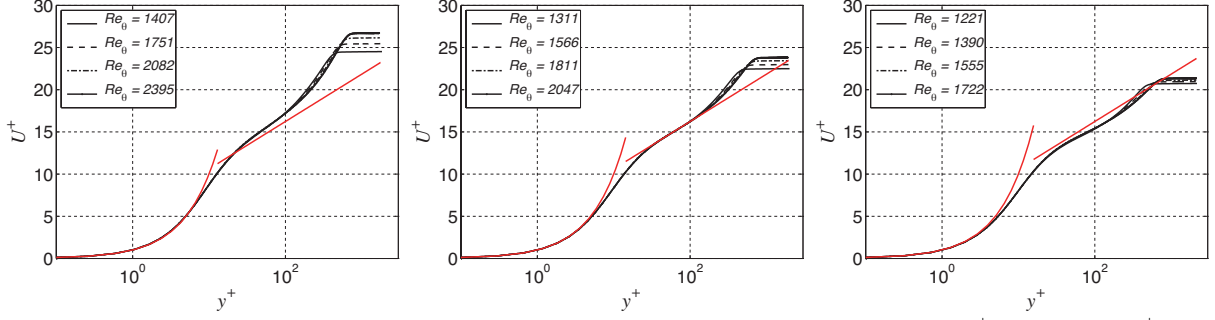


Figure 4: Profiles of mean streamwise velocity. Red solid lines show the linear and logarithmic ($U^+ = 1/0.41 \ln y^+ + 5$) velocity profile. Left, blowing; center, uncontrolled; right, suction.

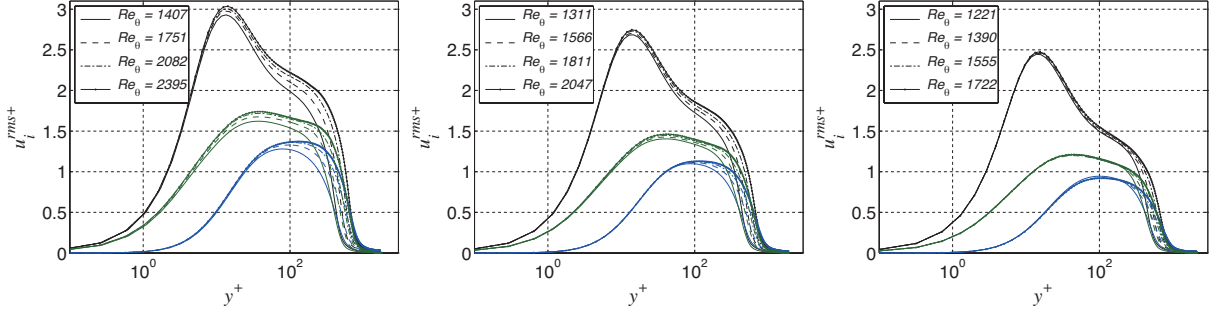


Figure 5: Profiles of a root-mean-square of velocity fluctuation. Left, blowing; center, uncontrolled; right, suction.

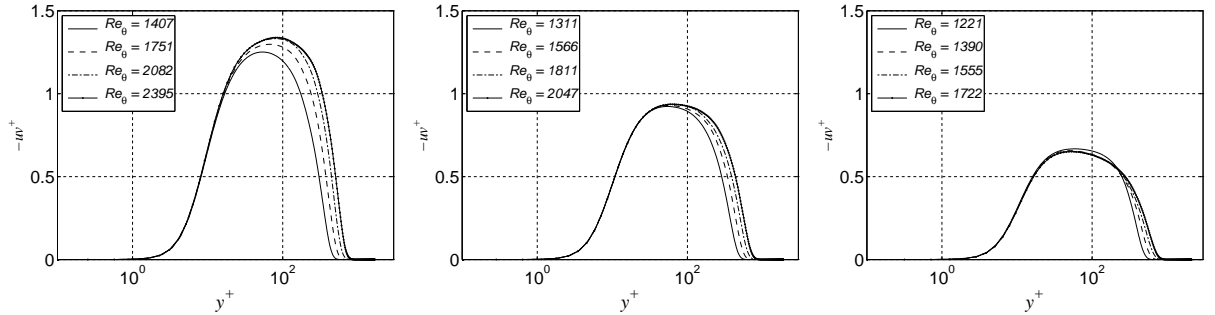


Figure 6: Profiles of Reynolds shear stress. Left, blowing; center, uncontrolled; right, suction.

the local wall units, the peaks in the blowing case develop downstream. The profiles of the suction case indicate that inner-scaling is observed throughout the inner layer as also evident for the Reynolds normal stresses.

4 Drag reduction by blowing

The effect of blowing or suction on the skin friction coefficient, $c_f = 2\tau_w/\rho U_\infty^2$, is plotted as function of the Reynolds number in Fig. 7, where ρ and τ_w denote density and wall-shear stress, respectively. The grey solid line shows the power-law distribution,

$$c_f = 0.024 Re_\theta^{-1/4}, \quad (2)$$

which indicates that all simulations have reached a developed turbulent state prior to the controlled region. Due to the variation of the boundary-layer thickness, the range of the Reynolds number differs among the cases. From the figure, the skin friction drag is reduced by blowing and enhanced by suction. Although the range of control is varied, it seems that the reduced

or enhanced profile of c_f approaches and collapses on a common line for the controlled cases.

The local drag reduction rate, R^L , net-energy saving rate, S^L , and control-gain are defined as

$$R^L(x) = \frac{c_{f,0} - c_f(x)}{c_{f,0}(x)}, \quad (3)$$

$$S^L(x) = \frac{c_{f,0}(x) - (c_f(x) + w_{in}(x))}{c_{f,0}(x)}, \quad (4)$$

$$G^L(x) = \frac{c_{f,0}(x) - c_f(x)}{w_{in}(x)} \quad (5)$$

where w_{in} denotes the local input power from the wall flux calculated as (detailed in Fukagata et al., 2009)

$$w_{in}(x) = \frac{1}{2} V_w(x)^3. \quad (6)$$

Due to the quite weak blowing amplitude, *i.e.* $w_{in}(x) \sim \mathcal{O}(10^{-9})$, the net-energy saving rate S^L is mostly equivalent to the drag reduction rate R^L . Figure 8 depicts S^L as a function of the Reynolds number of the uncontrolled case, $Re_{\theta,0}$. The profiles gradually increase with downstream distance. At the beginning of the blowing, S^L is approximately 13% but it

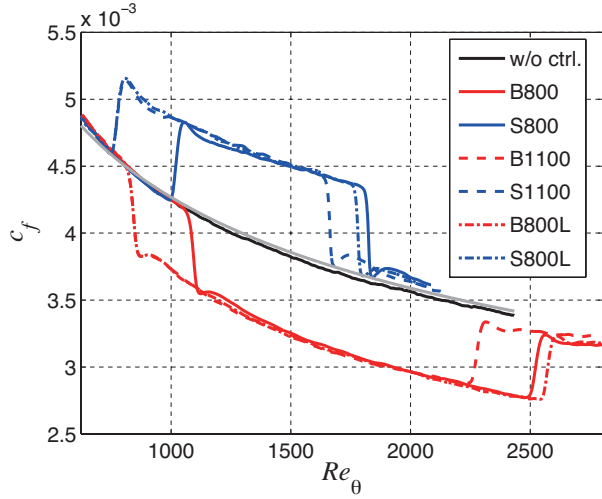


Figure 7: Friction coefficient as a function of Re_θ .

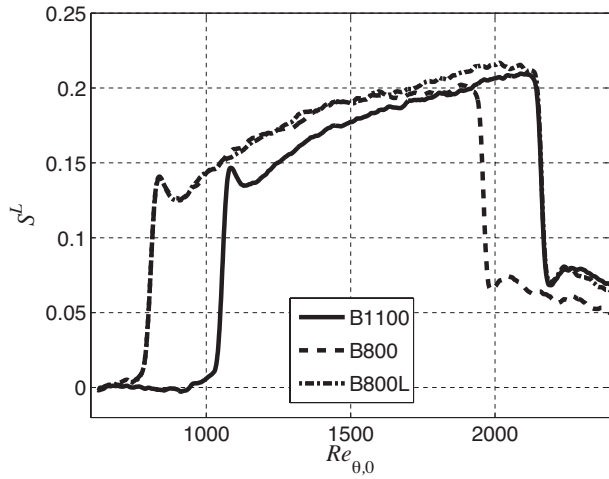


Figure 8: Local net-energy saving rate, S^L , as a function of $Re_{\theta,0}$.

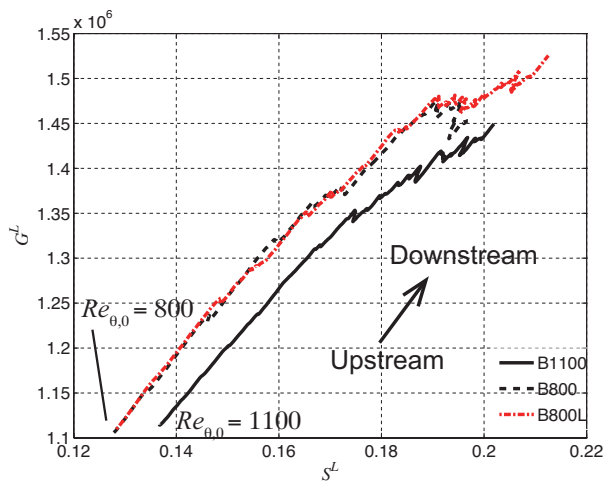


Figure 9: Local $S - G$ mapping.

increases up to over 20% at the end of the control region. The net-energy saving rate and the gain are plotted in Fig. 9 as a $S - G$ map, indicating that both the

net-energy saving rate and the control-gain increase with downstream development. Comparing B800 with B800L, it is clear that the larger blowing region results in a larger control efficiency. The other remarkable feature appears in the gap between B800 and B1100, where a later starting point yields less control-gain (or high net-energy saving rate) despite the equal blowing areas. This result indicates that in order to obtain a higher control-efficiency, 1) the long streamwise length of the blowing region and 2) the upstream location of the blowing-starting position are important factors. A jagged region of the profile further downstream is supposed to come from the division by the small value of input power in control-gain, G .

The mean net-energy saving rate S can be defined as $S = \frac{1}{x_e - x_s} \int_{x_s}^{x_e} S^L dx$, where x_s and x_e denote the streamwise location where blowing starts and end, respectively. From the present simulation, approximately 13% net-energy saving is achieved by blowing. Similarly the B1100, B800 and B800L cases achieve $S = 17.6\%$, 17.2% and 18.0% , respectively. Due to the growth of S^L , S is expected to increase as the blowing region is extended in streamwise direction. This fact indicates that a longer streamwise length of the uniform blowing continues to achieve larger drag reduction. The result of B800 and B1100 further indicates that the starting position of blowing, seems to affect the energy saving rate even though the area of the controlled region is equal; starting at higher Re_θ achieves a higher net-energy saving. However, this finding needs to be studied in more detail due to the comparably weak effect.

5 Physical decomposition of the friction drag

The Reynolds shear stress has been known to contribute to the skin friction since Fukagata et al. (2002) found an expression (FIK identity) for the componential contributions that different dynamical effects make to the skin friction drag. Here, the skin friction drag is decomposed into four terms as (see Fukagata et al., 2002),

$$\begin{aligned}
 c_f(x) &= c^\delta(x) + c^T(x) + c^D(x) + c^P(x) \quad (7) \\
 &= \frac{4(1 - \delta_d)}{Re_\delta} \\
 &\quad + 2 \int_0^1 2(1 - y) (-\overline{u'v'}) dy \\
 &\quad - 2 \int_0^1 (1 - y)^2 I_x dy \\
 &\quad - 2 \int_0^1 (1 - y)^2 \frac{\partial P}{\partial x} dy,
 \end{aligned}$$

where

$$I_x = \frac{\partial UU}{\partial x} + \frac{\partial \overline{u'u'}}{\partial x} + \frac{\partial UV}{\partial y} - \frac{1}{Re_\delta} \frac{\partial^2 U}{\partial x \partial x}. \quad (8)$$

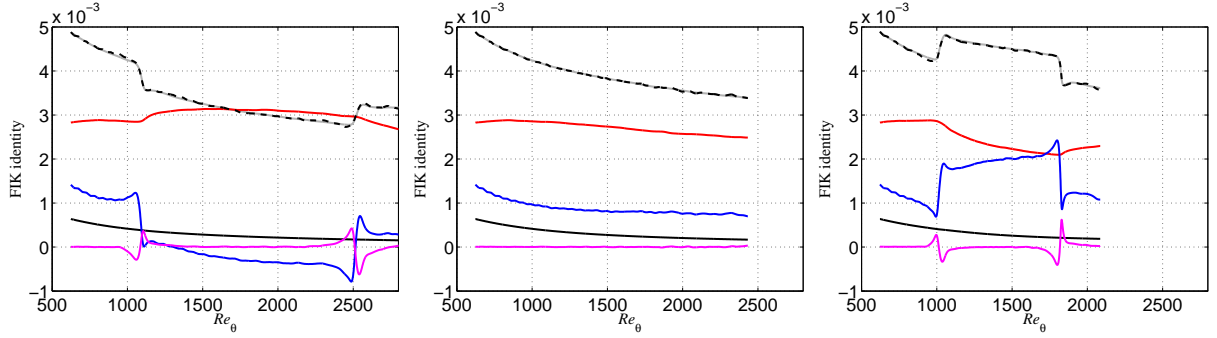


Figure 10: Decomposed skin friction drag. Left, blowing; center, uncontrolled; right, suction. Solid black, c^δ ; red, c^T ; blue, c^D ; magenta, c^P ; dashed black, FIK total; gray, c_f .

All terms are nondimensionalized by U_∞ and the 99% boundary layer thickness, δ . Here, δ_d denotes the displacement thickness. The terms on the right hand side are the contribution from the boundary layer thickness, the Reynolds shear stress, spatial development, and the pressure gradient, respectively. In the limit of high Reynolds numbers (for the uncontrolled case), the first term, c^δ , approaches zero because it is inversely proportional to the Reynolds number. The RSS term, c^T , and the spatial development term, c^D , has a large contribution on the skin friction drag in all cases, which are affected by control. The fourth term, c^P , is zero for zero-pressure-gradient conditions. This evaluation indicates that c^T and c^D are dominant in the skin friction drag. In the blowing and suction case with an infinite control region, however, the growth rate of the boundary layer is evaluated by the von Kármán equation with constant wall-normal velocity, written as

$$\frac{c_f}{2} = \frac{\partial \theta}{\partial x} - V_w. \quad (9)$$

In the blowing case, the skin friction is eliminated similarly to the uncontrolled case. From the Eq. (9),

$$\frac{\partial \theta}{\partial x} = V_w \quad (10)$$

is obtained. This indicates that the boundary layer thickness is supposed to grow at a constant rate at infinite Reynolds number. On the other hand, in the suction case, the boundary layer approaches an asymptotic boundary layer. From Eq. (9),

$$\frac{c_f}{2} = -V_w \quad (11)$$

follows. Figure 10 depicts the decomposed skin friction drag by using the FIK identity. The summation of all terms of the FIK identity agrees with the friction coefficient in all cases. Although a streamwise pressure-gradient is generated at the edge of the controlled region, it is eliminated over most part of the controlled region. Over the controlled region (without pressure gradient), the asymptotic features of the RSS term mentioned above can be confirmed in spite of the relatively low Reynolds number. As mentioned in

Kametani & Fukagata (2011), the drag reduction (enhancement) by blowing (suction) is dominantly due to the mean wall-normal flux in c^D . The profiles clearly show that c^D is a negative contribution in the blowing case, while it is a positive contribution in the suction case.

6 Spectral analysis

Pre-multiplied spanwise power spectra of the streamwise velocity fluctuation, $k_z \Phi_{uu}^z$, at $Re_{\theta,0} = 1800$ from B/S1100 cases are plotted in Fig. 11 as functions of wall-distance. The contour lines indicate that the energy is increased by blowing and decreased by suction. Blowing increases the small short wavelength component, suction decreases it. The profiles also indicate that blowing increases the energy near the wall, while suction decreases it. The range of wavelength and wall-distance of the spectra is spread by blowing, while suction has the opposite trend. A remarkable difference can be found at the comparably large scale components, $\lambda_z^+ \approx 60$, *i.e.* blowing enhances the fluctuation energy, while suction decreases it. Although the inner peak is increased by blowing and decreased by suction, the positions of them are mostly unaffected. These results indicate that the inner-region and outer region are differently affected by the controls. The effects of blowing and suction are more pronounced in the outer-layer. The turbulent fluctuation is enhanced by the wall flux induced from the wall. On the other hand, suction is supposed to stabilize the turbulence in the flow.

Similarly, the pre-multiplied cross spectra of u' and v' , $k_z \Phi_{uv}^z$ which corresponds the Reynolds shear stress is depicted in Fig. 12. In order to investigate the contribution to the skin friction drag, Φ_{uv}^z is weighted by the wall-distance. Blowing increases the spectra, while suction decreases it. As for small scale structures ($\lambda_z^+ < 4$), the turbulence near the wall is increased by blowing and decreased by suction. In the outer layer region, a second peak appears in the blowing case at $(\lambda_z^+, y^+) \approx (400, 100)$. This second peak indicates that, the large scale structures in the outer-region are enhanced by blowing. The contribution of

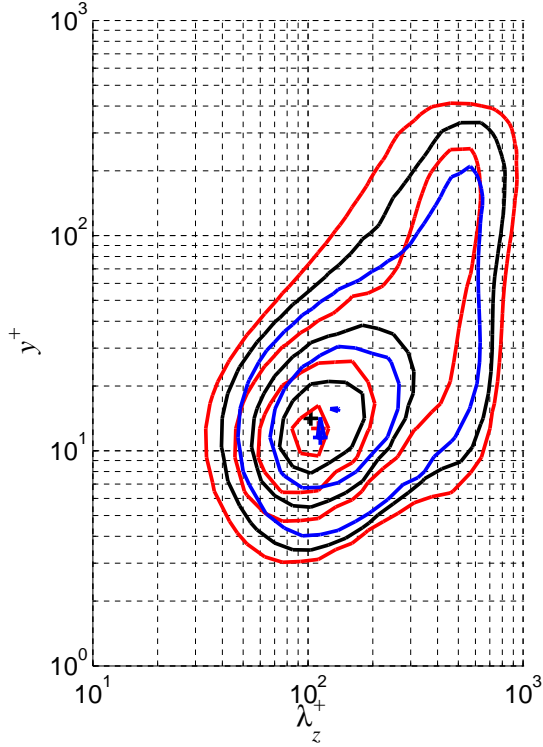


Figure 11: Spanwise pre-multiplied power spectra of u' at $Re_{\theta,0} = 1800$. Black, uncontrolled; red, blowing; blue, suction. Contour lines start from 1 with spacing of 1.

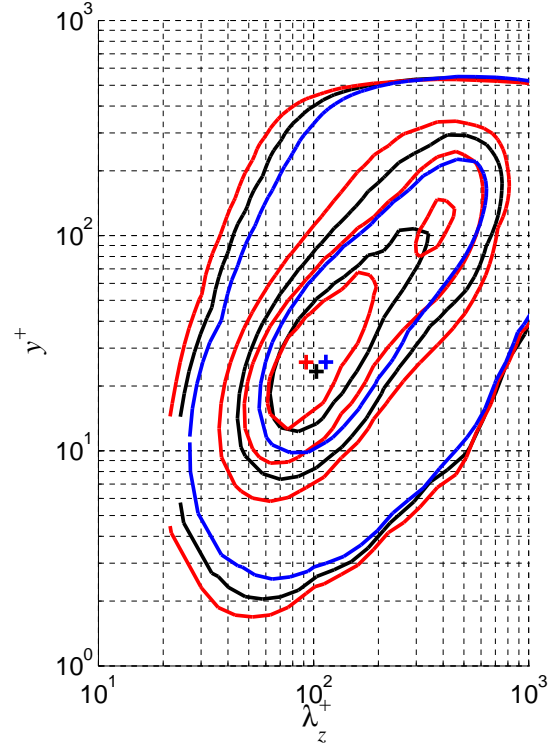


Figure 12: Spanwise pre-multiplied cross spectra of u' and v' at $Re_{\theta,0} = 1800$. Black, uncontrolled; red, blowing; blue, suction. Contour lines start from 0.2 spacing 0.2.

the large scale structure on the skin friction drag is generated by blowing. The effect of large scale structures in the uncontrolled case, however, is not confirmed due to the relatively low Reynolds number.

7 Conclusions

A large-eddy simulation of a spatially evolving turbulent boundary layer with uniform blowing and suction at moderate Reynolds number was performed. Similar to the low Reynolds number DNS by Kametani & Fukagata (2011), the skin friction drag reduction and enhancement by blowing and suction were confirmed, respectively. It is found that the local drag reduction rate is continuously growing in the downstream direction. From a map of the net-energy saving rate and the control-gain, the local control efficiency is found to increase in the downstream direction. Furthermore, the starting position of control located more upstream results in a higher net energy saving rate. This fact can indicate that higher drag reduction and control efficiency can be achieved as 1) the blowing region becomes wider and 2) the control starts at a more upstream location.

The decomposed skin fraction drag by the FIK identity and consideration of the Kármán momentum equation indicates the dominant terms of FIK iden-

tity in the high-Reynolds number turbulent boundary layer with and without blowing/suction. Although the boundary layer grows downstream, the spatial development term c^D : summation of the streamwise derivatives and mean convection, is negative in the blowing case, achieving friction drag reduction. In the suction case, c^D is the main factor of drag enhancement and, mostly, it balances with the Reynolds shear stress contribution, c^T .

The pre-multiplied power-spectra of the streamwise velocity fluctuation shows that the peak values are increased by blowing and decreased by suction. In the outer layer, the energy are remarkably affected by blowing and suction; blowing increases the energy, while suction decreases it. The pre-multiplied cross-spectra of the Reynolds shear stress weighted by the wall-distance show the contribution of the scale of turbulence, as mentioned in the FIK identity. The results show that blowing enhances the spectra, while suction reduces it. Similarly to the streamwise velocity power spectra, those in the outer-region are remarkably affected. In the blowing case, a second peak is generated. These structures are supposed to be more dominant at higher Reynolds numbers.

Acknowledgments

This project is financially supported by the Japan

Society for the Promotion of Science (JSPS). Computer time is provided by SNIC (Swedish National Infrastructure for Computing).

References

- Choi, H., Moin, P. and Kim, J. (1993), Direct numerical simulation of turbulent flow over riblets, *J. Fluid Mech.*, Vol. 255, pp. 503–539.
- Choi, H., Moin, P. and Kim, J. (1994), Active turbulent control for drag reduction in wall-bounded flows, *J. Fluid Mech.*, Vol. 262, pp. 75–110.
- Eitel-Amor, G., Örlü, R. and Schlatter, P. (2014), Simulation and validation of a spatially evolving turbulent boundary layer up to $Re_\theta = 8300$, *Int. J. Heat Fluid Flow*, Vol. 47, pp. 57–69.
- Fukagata, K., Iwamoto, K. and Kasagi, N. (2002), Contribution of Reynolds stress distribution to the skin friction in wall-bounded flows, *Phys. Fluids*, Vol. 14, pp. L73–L76.
- Fukagata, K., Sugiyama, K. and Kasagi, N. (2009), On the lower bound of net driving power in controlled duct flows, *Physica D*, Vol. 238-13, pp. 1082–1086.
- Kametani, Y. and Fukagata, K. (2011), Direct numerical simulation of spatially developing turbulent boundary layer with uniform blowing or suction, *J. Fluid Mech.*, Vol. 681, pp. 154–172.
- Kim, J., Moin, P. and Moser, R. (1987), Turbulence statistics in fully developed channel flow at low Reynolds number, *J. Fluid Mech.*, Vol. 177, pp. 133–166.
- Marusic, I., Mathis, R. and Hutchins, N. (2010), Predictive model for wall-bounded turbulent flow, *Science*, Vol. 329, pp. 193–196.
- Pirozzoli, S. and Bernardini, M. (2013), Proving high-reynolds-number effects in numerical boundary layers, *Phys. Fluids*, Vol. 25, 021704.
- Ricco, P. and Quadrio, M. (2008), Wall-oscillation conditions for drag reduction in turbulent channel flow, *Int. J. Heat Fluid Flow*, Vol. 29, pp. 601–612.
- Robinson, S.K. (1991), Coherent motions in the turbulent boundary layer, *Annu. Rev. Fluid Mech.*, Vol. 23, pp. 601–639.
- Spalart, P.R. (1988), Direct simulation of a turbulent boundary layer up to $Re_\theta = 1410$, *J. Fluid Mech.*, Vol. 187, pp. 61–98.
- Schlatter, P., Stolz, S. and Kleiser, L. (2004), LES of transitional flows using approximate deconvolution model, *Int. J. Heat Fluid Flow*, Vol. 25-3, pp. 549–558.
- Schlatter, P. and Örlü, R. (2010), Assessment of direct numerical simulation data of turbulent boundary layers, *J. Fluid Mech.*, Vol. 659, pp. 116–126.
- Schlatter, P. and Örlü, R. (2012), Turbulent boundary layers at moderate Reynolds numbers: inflow length and tripping effects, *J. Fluid Mech.*, Vol. 710, pp. 5–34.
- Schlatter, P., Li, Q., Örlü, R., Hussain, F., and Henningson, D.S. (2014), On the near-wall vortical structures at moderate Reynolds numbers, *Eur. J. Mech. B-Fluids*, Vol. 48, pp. 75–93.
- Sillero, J.A., Jimenez, J. and Moser, R.D. (2013), One-point statistics for turbulent wall-bounded flows at Reynolds number up to $\delta^+ \approx 2000$, *Phys. Fluids*, Vol. 25, 105102.
- Tomiyama, N. and Fukagata, K. (2013), Direct numerical simulation of drag reduction in a turbulent channel flow using spanwise traveling wave-like wall deformation, *Phys. Fluids*, Vol. 25, 105115.
- Türk, S., Daschiel, G., Stroh, A. and Frohnapfel, B. (2014), Turbulence statistics in fully developed channel flow at low Reynolds number, *J. Fluid Mech.*, Vol. 747, pp. 235–256.
- White, C. and Mungal, M. (2008), Mechanics and prediction of turbulent drag reduction with polymer additives, *Annu. Rev. Fluid Mech.*, Vol. 40, pp. 235–256.